

Performance of machine-learning-assisted Monte Carlo in sampling from simple statistical physics models

Luca Maria Del Bono,^{1,2} Federico Ricci-Tersenghi,^{1,2,3} and Francesco Zamponi¹

¹*Dipartimento di Fisica, Sapienza Università di Roma, Piazzale Aldo Moro 5, Rome 00185, Italy*

²*CNR-Nanotec, Rome unit, Piazzale Aldo Moro 5, Rome 00185, Italy*

³*INFN, sezione di Roma1, Piazzale Aldo Moro 5, Rome 00185, Italy*

Recent years have seen a rise in the application of machine learning techniques to aid the simulation of hard-to-sample systems that cannot be studied using traditional methods. Despite the introduction of many different architectures and procedures, a wide theoretical understanding is still lacking, with the risk of suboptimal implementations. As a first step to close this gap, we provide here a complete analytic study of the widely-used Global Annealing (also called Sequential Tempering) procedure applied to a shallow MADE architecture for the Curie-Weiss model. The contribution of this work is twofold: firstly, we give a description of the optimal weights and of the training under Gradient Descent optimization. Secondly, we compare what happens in Global Annealing with and without the addition of local Metropolis Monte Carlo steps. We are thus able to give theoretical insight into the best procedure to apply in this case. This work establishes a clear theoretical basis for the integration of machine learning techniques into Monte Carlo sampling and optimization.

I. INTRODUCTION

A. Setting and state-of-the-art

Obtaining configurations of hard-to-sample systems, such as spin glasses, amorphous solids and proteins, is a challenging task with both theoretical and practical applications [1–3]. The goal is to sample independent and identically distributed configurations from the Gibbs-Boltzmann (GB) distribution

$$P_{\text{GB}}(\boldsymbol{\sigma}) = \frac{e^{-\beta\mathcal{H}(\boldsymbol{\sigma})}}{\mathcal{Z}(\beta)}, \quad (1)$$

where $\boldsymbol{\sigma} = \{\sigma_1, \dots, \sigma_N\}$ is a set of N random variables describing the system, $\mathcal{Z}(\beta)$ is the partition function, $\mathcal{H}(\boldsymbol{\sigma})$ is the Hamiltonian and $\beta = 1/T$ is the inverse temperature.

Among the most widely used techniques are Parallel Tempering (PT) [4–6] and Population Annealing (PA) [7–11], which have established themselves as state-of-the-art approaches over the past few decades, remaining largely unchanged from their original formulations. In recent years, a new line of research aims to use machine-learning-assisted techniques to aid sampling. Stemming from the increasing capabilities of Generative Artificial Neural Networks, this line of research aims at using different kinds of architectures and frameworks, such as autoregressive models [12–15], normalizing flows [16, 17], diffusion models [18–20] and Boltzmann machines [21], to aid the sampling of statistical mechanics models. Methods inspired by theoretical physics techniques such as the Renormalization Group [22, 23] have been introduced and non-generative-based techniques can be used as well [24]. Moreover, similar techniques have been applied to the related task of finding the lowest energy configuration of statistical mechanics systems, a task with deep practical implications [25, 26]. At the same time, the Neural Network (NN) can also be used to obtain variational approximations to the GB distribution, thus improving over mean-field techniques, both in classical [14, 27] and quantum [28] systems.

One of the most widely used NN-based techniques is the Global Annealing (GA) procedure [13, 29], also called *Sequential Tempering* in the literature [29]. In GA, a set of M configurations is progressively cooled to lower temperatures. At each step, starting from M equilibrated configurations, a new series of configurations is generated using a neural network at a slightly lower temperature. The new configurations are equilibrated at the lower temperature, and the neural network is then retrained using the new equilibrated configurations as the starting point for the next step. Since the neural network produces entirely new configurations, the annealing procedure includes moves that can, in principle, update all the spins. Hence, the term *global*, to distinguish the updates from the single-variable local updates used in algorithms such as the classical Metropolis Monte Carlo. The original implementation of GA did not include the local steps and relied only on global moves (akin to an importance sampling) to equilibrate the newly generated configurations. While this procedure is exact if the thermalization is carried out for long enough times, in practice the time taken to achieve equilibrium can be very long.

The work of Gabrié *et al.* [30] has highlighted the importance of alternating global, NN-assisted moves and standard local Monte Carlo moves. In [30], the authors study the convergence properties of a NN-assisted Monte Carlo procedure

to a target distribution ρ^* . They provide numerical examples and analytical computations highlighting the faster convergence to ρ^* when local moves are alternated to the NN-based global ones. However, at variance with the standard GA procedure, in Ref. [30] no annealing in temperature is performed. The additional empirical evidence presented in subsequent studies [20, 31] underscores the need for physical intuition and a clear theoretical framework, both of which remain elusive in the context of the GA procedure.

B. Summary of results and outline of the work

In this work, we support the claim that local moves are necessary also in the context of GA by a complete theoretical analysis of the training and application of a shallow MADE (Masked Autoencoder for Distribution Estimation) neural network to assist sampling in the Curie-Weiss model. In particular, we focus on a single step of the Global Annealing procedure starting from the critical temperature of the model. This choice is motivated by the fact that in the Curie-Weiss model, this is the hardest temperature to work at, because the free energy at zero magnetization becomes locally flat (with vanishing first and second derivatives), which slows down equilibration. Immediately below, a pitchfork bifurcation happens, and two new states (the states with positive and negative magnetizations) appear. Being able to bypass the critical slowing down and correctly identify and follow the new states that appear upon lowering the temperature is generally the bottleneck in any annealing procedure; therefore, testing the Global Annealing at the critical temperature provides a good indication of the efficiency of the whole procedure.

More generally, we believe that this is an important first step towards understanding more complex systems, such as spin glasses, random optimization problems, and neural networks, in which flat directions in the (free) energy landscape play a very important role in the dynamical slowing down, especially in the low temperature region where a large number of states coexist [32–37].

Our main results are the following:

- We give a full analytical description of the shallow MADE architecture (Sec. III A 1: Eq. 13 and Fig. 1) and of its training dynamics (Sec. III A 3: Eq. 25 and Fig. 4) for the Curie-Weiss model, both for finite system sizes and in the thermodynamic limit;
- We show that a phenomenon akin to critical slowing down happens in learning at the critical temperature of the model (Sec. III A 3: Eq. 27), which once again highlights the special role played by this temperature as the bottleneck of the annealing;
- We study one step of the Global Annealing procedure when lowering the temperature starting at the critical point. We show (Sec. IV A: Fig. 8) that a perfectly trained network does not require local moves as long as the temperature step is small enough (i.e. scaling as the inverse of the square root of the system size). Instead, local moves are beneficial once a finite training time is taken into account (Sec. IV B: Fig. 9);
- We characterize the effectiveness of the Global Annealing procedure as compared to a standard local Metropolis Monte Carlo, in terms of first passage times in magnetization space (Sec. IV C: Fig. 10).

In particular, our work extends some of the results in Ref. [13], in which the shallow MADE architecture was only studied in the $N \rightarrow \infty$ limit. Although an exact architecture for sampling according to the GB distribution can be constructed [38], we focus here on a shallow MADE because it can be treated analytically also in the training process. Since training plays a crucial role in practical applications involving complex systems with unknown exact parameters, studying the shallow MADE architecture allows us to better control and analyze a setting that closely resembles real-world scenarios.

This paper is organized as follows. In Sec. II we give the background for our work. In particular, we introduce the Curie-Weiss model (II A) and the algorithms we study, local Metropolis Monte Carlo (II B 1) and NN-assisted Monte Carlo (II B 2) with a shallow MADE architecture (II C). In Sec. III we present a theoretical analysis of the training and of the NN-assisted Monte Carlo. In particular, we study the optimal model and the training dynamics (III A); moreover, we compare the performance of the algorithms in terms of first-passage times in magnetization space (III B). In Sec. IV we apply these methods to compare different sampling procedures. We first consider Global Annealing with a fully trained machine, with and without local MC steps (IV A); then, we study how the scenario changes when one takes into account a finite training time (IV B); additionally we compare Global Annealing with vanilla Metropolis Monte Carlo (IV C). Finally, in Sec. V we draw our conclusions and highlight some possible future developments.

II. BACKGROUND

A. The Curie-Weiss model

In this paper, we consider the simplest model of ferromagnetic phase transitions, the Curie-Weiss (CW) model. In the CW model, the state of the system is given by a set of N Ising variables, $\boldsymbol{\sigma}$, $\sigma_i = \pm 1$, $i = 1, \dots, N$. The Hamiltonian reads:

$$\mathcal{H}(\boldsymbol{\sigma}) = -\frac{N}{2}m(\boldsymbol{\sigma})^2, \quad (2)$$

where $m(\boldsymbol{\sigma}) = \frac{1}{N} \sum_i \sigma_i$ is the (intensive) magnetization of the system. It is well known that this model undergoes a phase transition in the thermodynamic limit at a critical temperature $T_c = 1$, passing from a disordered paramagnetic phase at $T > 1$ to an ordered ferromagnetic phase at $T < 1$ (see Chapter 2 of [39] for a pedagogical introduction). In the ferromagnetic phase, the model develops a non-trivial spontaneous equilibrium magnetization, which is given by the non-zero solution m^* of the equation

$$m^* = \tanh(\beta m^*). \quad (3)$$

The model can be simulated using one of many different algorithms. We focus on classical local Metropolis Monte Carlo, a standard Swiss-knife algorithm for the simulation of statistical physics systems, and on a NN-assisted Monte Carlo procedure, Global Annealing. In particular, we want to study which algorithm is faster in equilibrating the system at $T < 1$ starting from $T = T_c = 1$, as measured using as a proxy the time needed to first reach the equilibrium magnetization that solves Eq. (3). In the next section, we describe in detail the algorithms that we considered in our analysis.

B. Algorithms

1. Standard local Metropolis Monte Carlo

In the standard local Metropolis Monte Carlo (LMMC) [40] algorithm, one performs a series of local, single-spin-flip moves. A single Monte Carlo ‘step’ consists of the following operations, starting from a configuration $\boldsymbol{\sigma}(t) = \boldsymbol{\sigma}$ at time t :

1. propose a new configuration by flipping the spin of a randomly chosen site, $\sigma_i \rightarrow -\sigma_i$;
2. calculate the energy difference, $\Delta E = -2 \left[\frac{1}{N} - \sigma_i m(\boldsymbol{\sigma}) \right]$, between the new configuration and the current configuration;
3. accept the move, i.e. set $\boldsymbol{\sigma}(t+1) = \boldsymbol{\sigma}'$ where $\boldsymbol{\sigma}'$ is obtained from $\boldsymbol{\sigma}$ by flipping σ_i , with probability:

$$\text{Acc}[\boldsymbol{\sigma} \rightarrow \boldsymbol{\sigma}'] = \min [1, e^{-\beta \Delta E}] .$$

Otherwise, reject the move and set $\boldsymbol{\sigma}(t+1) = \boldsymbol{\sigma}$.

N such steps are commonly referred to as a Monte Carlo Sweep (MCS). It is easy to see that the computational complexity of a MCS is $\mathcal{O}(N)$.

Although LMMC frequently serves as a building block for more advanced and powerful algorithms, such as Parallel Tempering [4] and Population Annealing [7, 10, 41], it may encounter limitations when employed in isolation. For instance, it can remain trapped for long times in (local) minima of the free energy landscape, thus failing to sample effectively the whole space of configurations.¹

¹ For instance, in the CW model below T_c , LMMC can remain stuck in the state with positive (negative) magnetization. Escaping the state and reaching the state with negative (positive) magnetization requires a time growing exponentially with the size of the system N .

2. The Global Annealing procedure

The main disadvantage of the LMMC algorithm described in the previous section is that it can only perform local moves. A recently proposed solution is to use a generative NN to propose global moves. The idea is to start from a configuration σ and use a generative NN to generate a whole new configuration σ' of the system, which is then accepted with an acceptance ratio Acc chosen in order to satisfy detailed balance:

$$\text{Acc}[\sigma \rightarrow \sigma'] = \min \left[1, \frac{P_{\text{GB}}(\sigma') \times P_{\text{NN}}(\sigma)}{P_{\text{GB}}(\sigma) \times P_{\text{NN}}(\sigma')} \right], \quad (4)$$

where $P_{\text{NN}}(\sigma)$ is the probability that the NN generates the configuration σ . Note that in this case the whole configuration is updated in a single operation, which then corresponds roughly to a Monte Carlo Sweep. While this strategy is essentially equivalent to an importance sampling of $P_{\text{GB}}(\sigma)$ using $P_{\text{NN}}(\sigma)$ as a generator, the formulation in terms of a stochastic process with an acceptance ratio allows one to combine the global moves with local ones, as we will do in the following.

The success of this strategy relies on the ability of the NN to generate configurations close to the ones at equilibrium, so that the full configuration space is well sampled and the acceptance rate is not too low. It has been shown [15, 38] that it is possible to design networks that are powerful enough to sample according to the GB distribution. The question then becomes whether one is able to train such networks in practice. While variational procedures that do not require sampling have been used [27], we focus here on methods that use previously generated equilibrium configurations to train the model, because variational methods have been shown to be prone to mode collapse in complex problems [13].

In these approaches, the NN is first trained at a temperature β using a set of M equilibrium configurations. The training can be carried out, for instance, by maximizing the model likelihood of the available M equilibrium configurations. Then, the NN is used to generate a new series of configurations, which are then used as proposal moves for a global Monte Carlo. The training set is updated using the acceptance rate in Eq. (4) and the model is trained again. Unfortunately, obtaining the M configurations used to train the model can be complicated, especially if one is interested in the low-temperature, hard-to-sample regime of a model. And of course, if we are already able to obtain equilibrium configurations, there is no interest in developing new sampling methods. A solution to both issues is to use the Global Annealing (GA) procedure, an annealing procedure that uses the self-consistently trained NN in order to generate configurations at lower and lower temperatures.

In GA, the NN is first trained using M configurations at a high temperature, at which it is easy to sample configurations at equilibrium (for example via LMMC). Then, the NN is used at inverse temperature $\beta' = \beta + \Delta\beta > \beta$ to propose a new set of M configurations at β' by performing θ_{global} global moves. This new set of configurations is then used to train a new NN (or retrain the previous one). The whole procedure can then be repeated until the desired temperature is reached. The general scheme of GA is summarized in Algorithm 1. Additionally, θ_{local} LMMC steps can be alternated to the global moves proposed by the NN (steps 9-11 of Alg. 1) but not all implementations include them [13, 29]. Understanding the importance of performing local moves is one of the goals of this paper.

Algorithm1 Global Annealing

- 1: **Input:** Initial inverse temperature β_{start} , final inverse temperature β_{end} , temperature step $\Delta\beta$, number of configurations M , number of global steps per temperature θ_{global} , number of local steps per global step θ_{local} .
 - 2: **Initialize:** A set of M equilibrium configurations at β_{start} (sampled e.g. using standard Metropolis MC)
 - 3: **while** $\beta < \beta_{\text{end}}$ **do**
 - 4: Train a neural network (NN) using the set of M configurations
 - 5: Lower the temperature: $\beta \leftarrow \beta + \Delta\beta$
 - 6: **for** m in $1, \dots, M$ **do**
 - 7: Choose the m -th configuration from the set as the initial state
 - 8: **for** t in $1, \dots, \theta_{\text{global}}$ **do**
 - 9: Propose a new configuration using the NN
 - 10: Accept or reject the configuration with probability (4) at the new temperature $T = 1/\beta$
 - 11: **for** t in $1, \dots, \theta_{\text{local}}$ **do**
 - 12: Perform a LMMC step
 - 13: **end for**
 - 14: **end for**
 - 15: **end for**
 - 16: **end while**
-

The GA scheme is quite general. The specific implementation then requires the choice of a generative NN. In this paper, we consider a shallow MADE, as described in the next section.

C. The MADE architecture

We consider as our architecture of choice the shallow MADE (Masked Autoencoder for Distribution Estimation, [42]) considered in Ref. [13].

The MADE is an autoregressive model, in which the probability of a configuration is represented as a sequence of conditional probabilities:

$$P_{\text{NN}}(\boldsymbol{\sigma}) = P(\sigma_1)P(\sigma_2 | \sigma_1)P(\sigma_3 | \sigma_1, \sigma_2) \cdots P(\sigma_N | \sigma_1, \cdots, \sigma_{N-1}) = \prod_{i=1}^N P(\sigma_i | \boldsymbol{\sigma}_{<i}), \quad (5)$$

and the $P(\sigma_i | \boldsymbol{\sigma}_{<i})$ are written in terms of a set of parameters that defines the model. This formalization allows us not only to compute the probability of a given configuration $\boldsymbol{\sigma}$, but also to generate a new one from scratch in polynomial time using *ancestral sampling*. In ancestral sampling, first the spin σ_1 is generated using $P(\sigma_1)$, then σ_2 is generated using σ_1 according to $P(\sigma_2 | \sigma_1)$, then σ_3 is generated using σ_2 and σ_3 according to $P(\sigma_3 | \sigma_1, \sigma_2)$ and so on.

Specifically, the shallow MADE we are considering parametrizes the probability as $P(\sigma_1) = 1/2$ and, for $i > 1$,

$$P(\sigma_i | \boldsymbol{\sigma}_{<i}) = \frac{\exp\left(\sum_{j=1}^{i-1} J_{ij} \sigma_i \sigma_j\right)}{2 \cosh\left(\sum_{j=1}^{i-1} J_{ij} \sigma_j\right)} \quad (6)$$

where J_{ij} are learnable weights. We make a further simplification, motivated by permutation invariance of the original model, that the weights are shared across each row, so that $J_{ij} = J_i$ and

$$P(\sigma_i | \boldsymbol{\sigma}_{<i}) = \frac{\exp\left(\sum_{j=1}^{i-1} J_i \sigma_i \sigma_j\right)}{2 \cosh\left(\sum_{j=1}^{i-1} J_i \sigma_j\right)} = \frac{\exp(J_i \sigma_i M_{<i})}{2 \cosh(J_i M_{<i})}, \quad (7)$$

where $M_{<i}(\boldsymbol{\sigma}_{<i}) = \sum_{j=1}^{i-1} \sigma_j$. This architecture corresponds to a NN with a single dense autoregressive layer with shared per-row weights (i.e. all the weights for each row are the same, so that, in practice, for each conditional probability one sums the previous input variables and then multiplies the sum by a single learnable weight), followed by a softmax activation function, and is fully specified by a set of $N - 1$ weights $\underline{J} = (J_2, \cdots, J_N)$, that is, a number of parameters linear in the system size. This setup differs from what is usually applied in deep learning, in which networks have a large number of parameters, a feature that seem to be connected to their ability to be trained to reach good generalization even in situations in which the loss is strongly nonconvex (the interested reader can refer to [36, 37] and references therein). While the shallow MADE architecture cannot leverage the properties of deep NNs, the problem at hand is simple enough that this architecture is adequate [13]. Moreover, as explained in Sec. III A, the best set of parameters of the model can be found by maximizing the likelihood of the training data and for this shallow MADE applied to the Curie-Weiss model this optimization can be written down explicitly, as we do in the next section. This allows us to get insight that can be applied to more complicated architectures, as well to more complex physical systems, whose study is left to future work.

III. METHODS

A. Analysis of the MADE architecture

1. Optimal values of the weights

In order to analyze the MADE architecture described in Sec. II C, let us start by introducing the cross entropy S_c between P_{GB} and P_{MADE} for a set of weights \underline{J} ,

$$\begin{aligned} S_c(\underline{J}) &= - \sum_{\{\boldsymbol{\sigma}\}} P_{\text{GB}}(\boldsymbol{\sigma}) \log P_{\text{MADE}}(\boldsymbol{\sigma}) = - \sum_{\{\boldsymbol{\sigma}\}} P_{\text{GB}}(\boldsymbol{\sigma}) \log \left[\frac{1}{2} \prod_{i=2}^N P(\sigma_i | \boldsymbol{\sigma}_{<i}) \right] \\ &= N \log 2 - \sum_{i=2}^N \sum_{\{\boldsymbol{\sigma}\}} P_{\text{GB}}(\boldsymbol{\sigma}) \{ J_i \sigma_i M_{<i} - \log[\cosh(J_i M_{<i})] \} . \end{aligned} \quad (8)$$

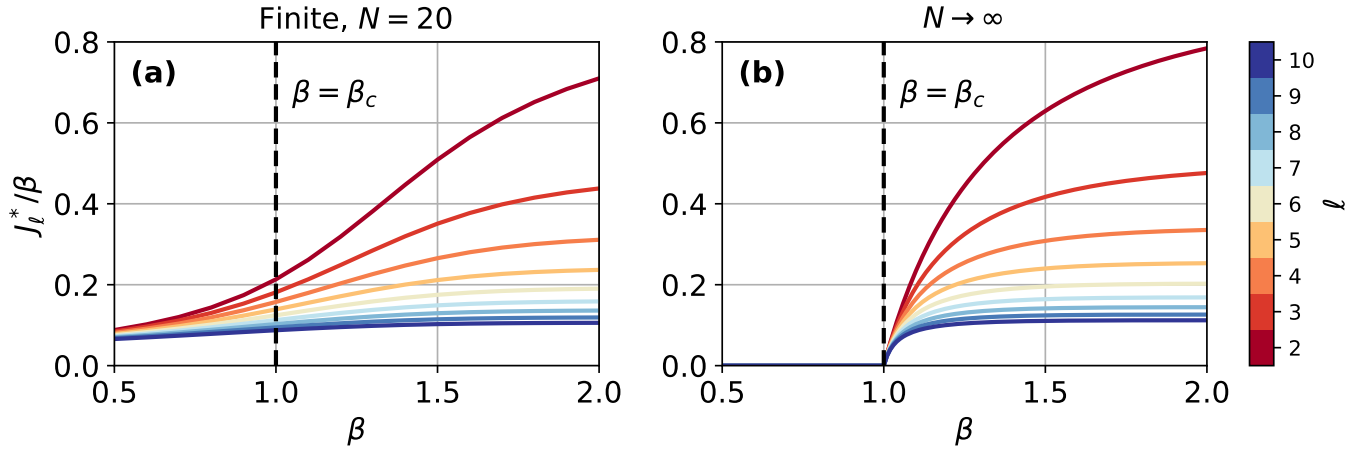


FIG. 1. Behavior of the optimal couplings J_ℓ^*/ℓ as a function of β for $\ell \leq 10$. (a) Finite N , ($N = 20$), obtained solving Eq. (11). (b) Infinite N , obtained solving Eq. 14.

The sum over σ runs over all 2^N possible configurations of the system. Minimizing the cross entropy with respect to the ℓ -th coupling J_ℓ yields:

$$\sum_{\{\sigma\}} P_{\text{GB}}(\sigma) M_{<\ell} \sigma_\ell = \sum_{\{\sigma\}} P_{\text{GB}}(\sigma) M_{<\ell} \tanh(J_\ell M_{<\ell}) . \quad (9)$$

In the CW model, the sum over the 2^N spin configurations can be reduced to a polynomial sum by rewriting the Gibbs-Boltzmann distribution P_{GB} in Eq. (1) with the CW Hamiltonian in Eq. (2) via a Hubbard-Stratonovich transformation as:

$$P_{\text{GB}}(\sigma) = \frac{1}{\hat{\mathcal{Z}}(\beta)} \int dh e^{-\frac{Nh^2}{2\beta}} e^{h \sum_i \sigma_i} , \quad (10)$$

where $\hat{\mathcal{Z}}(\beta) = \mathcal{Z}(\beta) \sqrt{\frac{2\pi\beta}{N}}$ is the new normalizing constant. Inserting this expression in Eq. (9) one finds:²

$$\int dh e^{-\frac{Nh^2}{2\beta}} \sinh(h) \cosh^{N-\ell}(h) \Sigma_1(h) = \int dh e^{-\frac{Nh^2}{2\beta}} \cosh^{N-\ell+1}(h) \Sigma_2(h, J_\ell) , \quad (11)$$

where

$$\Sigma_1(h) = \sum_{\substack{M=-(\ell-1) \\ M+=2}}^{\ell-1} \binom{\ell-1}{\frac{\ell-1-M}{2}} e^{hM} M \quad \text{and} \quad \Sigma_2(h, J_\ell) = \sum_{\substack{M=-(\ell-1) \\ M+=2}}^{\ell-1} \binom{\ell-1}{\frac{\ell-1-M}{2}} e^{hM} M \tanh(J_\ell M) , \quad (12)$$

where the magnetization M increases in steps of 2 in the sums. Note that with some manipulations, Eq. (11) can be simplified to³

$$2^{\ell-1}(\ell-1) \int dh e^{-\frac{Nh^2}{2\beta}} \sinh^2(h) \cosh^{N-2}(h) = \int dh e^{-\frac{Nh^2}{2\beta}} \cosh^{N-\ell+1}(h) \Sigma_2(h, J_\ell) . \quad (13)$$

The latter equations involve a single integral and a sum over a linear number of terms in N , and can thus be solved numerically to find the optimal values of the weights J_ℓ . An example of the behavior of J_ℓ as a function of β is shown in Fig. 1a.

² The result follows from explicitly computing the sums over the spins $\geq \ell$ while rewriting the sums over spins $< \ell$ in terms of sums over the possible magnetizations.

³ The simplification comes from the fact that the sum that defines Σ_1 can be computed explicitly and yields:

$$\Sigma_1(h) = \sum_{\substack{M=-(\ell-1) \\ M+=2}}^{\ell-1} \binom{\ell-1}{\frac{\ell-1-M}{2}} e^{hM} M = \sum_{k=0}^{\ell-1} \binom{\ell-1}{k} e^{h(\ell-1-2k)} (\ell-1-2k) = 2^{\ell-1}(\ell-1) \cosh^{\ell-2}(h) \sinh(h).$$

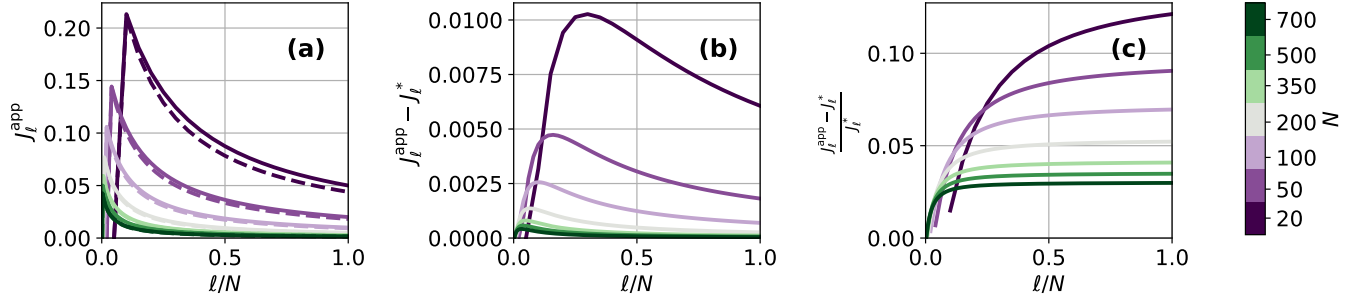


FIG. 2. Comparison at $\beta = \beta_c = 1$ of the approximated couplings J_ℓ^{app} as found by solving Eq. (16) with the exact ones. (a) J_ℓ^{app} (dashed) compared with the exact J_ℓ^* (full). (b) Absolute error $J_\ell^* - J_\ell^{\text{app}}$. (c) Relative error $(J_\ell^* - J_\ell^{\text{app}})/J_\ell^*$.

2. Thermodynamic limit

In the $N \rightarrow \infty$ limit the integrals over h can be evaluated using the Laplace method, and Eq. (11) reduces to

$$\Sigma_2(h^*, J_\ell) = \Sigma_1(h^*) \tanh(h^*), \quad (14)$$

where h^* is the solution of the saddle-point equation

$$h^* = \beta \tanh(h^*). \quad (15)$$

Notice that we can consider just the positive solution for h^* , since taking into account the negative one simply yields additional factors of two on both sides of the equations. These results match the equations derived in Ref. [13] for the $N \rightarrow \infty$ limit. An example of the behavior of the weights in the infinite- N limit is shown in Fig. 1b.

For $\beta \leq \beta_c = 1$, Eq. (15) only admits the $h^* = 0$ solution. As a consequence, $J_\ell = 0 \forall \ell$, i.e. for $N \rightarrow \infty$ all the weights vanish. We can then try a small J_ℓ approximation of Eq. (11) at finite N . At first order, this yields the equation:

$$J_\ell^{\text{app}} = \frac{\int_{-\infty}^{\infty} \exp\left(-\frac{N}{2\beta}h^2\right) \cosh^{N-2}(h) \sinh^2(h) dh}{\int_{-\infty}^{\infty} \exp\left(-\frac{N}{2\beta}h^2\right) \cosh^{N-2}(h) \left((\ell-2) \sinh(h)^2 + \cosh(h)^2\right) dh}. \quad (16)$$

A comparison between the approximated weights and the exact ones is shown in Fig. 2. In the following section, we study how the weights of the model are learned during training.

3. Training dynamics

We consider a gradient descent (GD) training dynamics, taking as a loss the cross entropy defined in Eq. (8). Then, the update rule of the parameters can be written as:

$$J_\ell^{(t+1)} = J_\ell^{(t)} - \eta_\ell \nabla_\ell S_c(\underline{J}^{(t)}), \quad (17)$$

where η_ℓ is the learning rate for the ℓ -th weight and the gradient is:

$$\nabla_\ell S_c(\underline{J}) = \frac{2^{N-\ell}}{\mathcal{Z}(\beta)} \sqrt{\frac{2N}{\pi\beta}} \int_{-\infty}^{\infty} dh e^{-\frac{Nh^2}{2\beta}} \cosh(h)^{N-\ell} \sum_{\substack{M=-(\ell-1) \\ M+=2}}^{\ell-1} \binom{\ell-1}{\frac{\ell-1-M}{2}} e^{hM} M [\cosh(h) \tanh(J_\ell M) - \sinh(h)]. \quad (18)$$

Note that because the cross entropy is a sum of terms, each involving a single weight, the gradient $\nabla_\ell S_c(\underline{J})$ depends only on J_ℓ and the gradient descent dynamics of different weights are decoupled.

In the continuous time limit (gradient flow), Eq. (17) reads:

$$\dot{J}_\ell = -\eta_\ell \nabla_\ell S_c(\underline{J}). \quad (19)$$

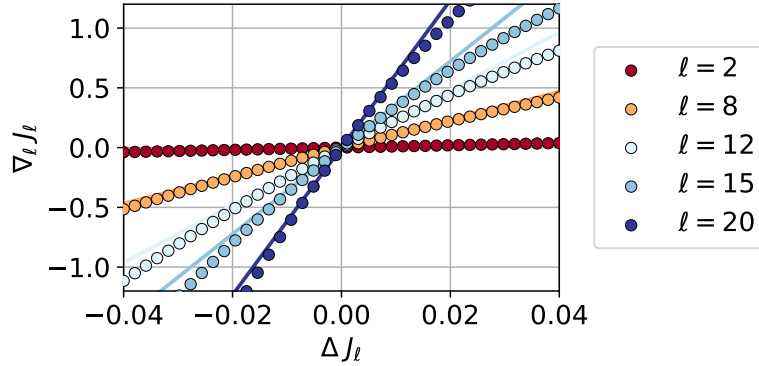


FIG. 3. Comparison between the gradients obtained by linearizing around the optimal solution J_ℓ^* (full lines) and the gradients computed using `pytorch` backpropagation on a large dataset (data points) as a function of the distance from the optimal couplings, $\Delta J_\ell = J_\ell - J_\ell^*$. Details: $N = 20$ spins, $\beta = 1$, the dataset is made of $5 \cdot 10^6$ configurations obtained by starting at infinite temperature and then performing 30 MCS at $\beta = 1$.

The gradient can be linearized around the solution J_ℓ^* of Eq. (11), yielding:

$$\dot{J}_\ell = -\eta_\ell \Delta J_\ell \mathbb{H}_\ell(J_\ell^*), \quad (20)$$

where $\Delta J_\ell = J_\ell - J_\ell^*$ is the difference with respect to the optimal couplings and \mathbb{H}_ℓ is the second derivative of the cross entropy, given by:

$$\mathbb{H}_\ell(J_\ell) = \frac{2^{N-\ell}}{\mathcal{Z}(\beta)} \int_{-\infty}^{\infty} dh e^{-\frac{Nh^2}{2\beta}} \sqrt{\frac{2N}{\pi\beta}} \cosh(h)^{N-\ell+1} \sum_{\substack{M=-(\ell-1) \\ M+=2}}^{\ell-1} \binom{\ell-1}{\frac{\ell-1-M}{2}} e^{hM} M^2 \operatorname{sech}^2(J_\ell M). \quad (21)$$

A comparison between the linearized gradient and the true gradient is shown in Fig. 3, highlighting the very good agreement between the two.

Unfortunately, this approach is not easily tractable analytically. Instead, for $\beta \leq \beta_c = 1$, we can consider the small J_ℓ^* approximation and linearize around zero. By linearizing Eq. (19) (in the small J_ℓ^* approximation), one finds:

$$\dot{J}_\ell = -\eta_\ell [\langle M_{<\ell} \sigma_\ell \rangle - \mathbb{H}_\ell(0) J_\ell] = -\eta_\ell [(\ell-1)c_N - \mathbb{H}_\ell(0) J_\ell], \quad (22)$$

where $\mathbb{H}_\ell(0)$ has now the simple form:

$$\mathbb{H}_\ell(0) = (\ell-1)[1 + (\ell-2)c_N], \quad (23)$$

and c_N is the two-spin correlation function $c_N = \langle s_i s_j \rangle$, $i \neq j$ between any two different spins,

$$c_N = \langle s_i s_j \rangle = \frac{\int_{-\infty}^{\infty} e^{-\frac{Nh^2}{2\beta}} \sinh^2(h) \cosh^{N-2}(h) dh}{\int_{-\infty}^{\infty} e^{-\frac{Nh^2}{2\beta}} \cosh^N(h) dh}, \quad (24)$$

which decays as $1/N$ for $T < 1$ and as $1/\sqrt{N}$ at $T = 1$. The latter approximation allows for the training dynamics to be solved explicitly:

$$J_\ell(t) = c_N \tau_\ell (\ell-1) \left[1 - e^{-\frac{\eta_\ell t}{\tau_\ell}} \right], \quad (25)$$

where the characteristic time τ_ℓ is simply the inverse of the Hessian, $\tau_\ell = 1/\mathbb{H}_\ell(0)$, and η_ℓ is the learning rate. Notice that the prefactor $J_\ell^{\text{app}} = c_N \tau_\ell (\ell-1) = c_N / (1 + (\ell-2)c_N)$ corresponds exactly to the small J_ℓ approximation derived in Eq. (16). While this argument can probably be made more rigorous, e.g. using the Polyak–Łojasiewicz inequality, we instead verify the correctness of this assumption numerically in Fig. 4, finding an excellent agreement between the exact and approximate solutions.

Equation (25) allows to predict several important trends:

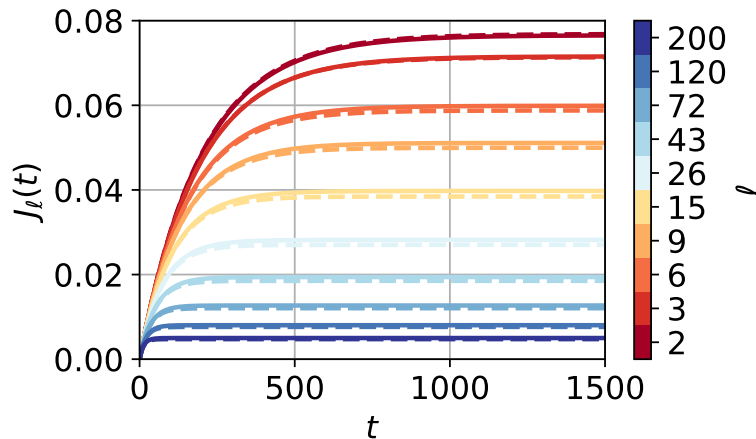


FIG. 4. Comparison between the training of the weights obtained by the approximation in Eq. (25) (full lines) and the training performed numerically using `pytorch` over a large dataset. Details: $N = 200$ spins, $\beta = 1$, the dataset is made of $5 \cdot 10^6$ equilibrium configurations, learning rate $\eta_\ell = 1/[N(\ell - 1)]$.

- the relative error vanishes exponentially in time, as $\frac{|\Delta J_\ell|}{J_\ell} = e^{-\frac{\eta_\ell t}{\tau_\ell}}$;
- if $\eta_\ell = 1/[N(\ell - 1)]$ then $\frac{|\Delta J_\ell|}{J_\ell} = e^{-\frac{1+(\ell-2)c_N}{N}t} = A(t, N)e^{-\frac{\ell}{\lambda(t, N)}}$, where $\log A(t, N) = \frac{t}{N}(2c_N - 1)$ and $\lambda(t, N) = \frac{N}{tc_N}$; hence, the relative error also vanishes exponentially in ℓ at fixed time;
- again, if $\eta_\ell = 1/[N(\ell - 1)]$, then the effective time scale is $\hat{\tau}_\ell = \frac{\tau_\ell}{\eta_\ell} = \frac{N}{1+(\ell-2)c_N}$.

These predictions are verified in Fig. 5.

Notice that Eq. (25) requires to specify the learning rate η_ℓ for weight ℓ . From a discretization of the gradient flow Eq. (25), noticing that in GD one performs a single discrete step at each time so that the minimum increment in t is one, it follows that the learning rate must be taken as

$$\eta_\ell \sim \tau_\ell = 1/H_\ell(0). \quad (26)$$

This result matches the known one for convex optimization problems [43]. Indeed, this choice allows one to learn all the weights in a time $\mathcal{O}(1)$. However, this requires the knowledge of the Hessian, which is not usually known, and the choice in Eq. (26) is therefore unrealistic.

In a more realistic implementation (at least for simple GD optimization), which we therefore consider in the following, one would use a single learning rate η for all the weights. Then, the prescription for smooth convergence in Eq. (26) becomes

$$\eta \leq \tau_N \sim \frac{1}{c_N N^2}, \quad (27)$$

because the learning rate must be smaller than the smallest timescale in order for all the weights to be able to converge. At the critical temperature $T = T_c$, since $c_N \sim \frac{1}{\sqrt{N}}$ (see, for instance, Ref. [44, Eq. 23]), we need $\eta \sim N^{-\frac{3}{2}}$, which is the learning rate we will consider in the following. Notice that, since the slowest timescale (corresponding to $\ell = 2$) is of order 1, the effective timescale to learn all the weights goes as $N^{\frac{3}{2}}$. On the other hand, for $T \geq T_c$ (that is when we are no longer in the critical regime), $c_N \sim \frac{1}{N}$ and therefore the maximum learning rate that can be chosen goes as $\eta \sim \frac{1}{N}$, so that the timescale to learn all the weights is $\mathcal{O}(N)$ (see Fig. 6). Therefore, at criticality, proper training requires an additional factor \sqrt{N} in training time. This factor is exactly the same that appears due to critical slowing down (with exactly the same dynamical critical exponent) when performing Glauber dynamics or Metropolis-Hastings Monte Carlo [45]. So, in this setting, the hardness of sampling at criticality is instead transferred to the training.⁴ It would be interesting to verify whether this scenario is generically present for different models and

⁴ Notice that we can rewrite the scaling of the learning rate around the critical temperature using a scaling function. In particular, we can write $\eta = N^{-3/2}f(\sqrt{N}\Delta T)$, where $\Delta T = T - T_c$, $f(0) = 1$ and $f(x) \sim x$ for $x \rightarrow \infty$. Therefore, the effect of criticality can be felt inside a window of size $1/\sqrt{N}$. As we will see in Sec. IV A, this is the natural scaling of the temperature steps in the annealing procedure, so one cannot avoid the critical region by simply taking a larger temperature step.

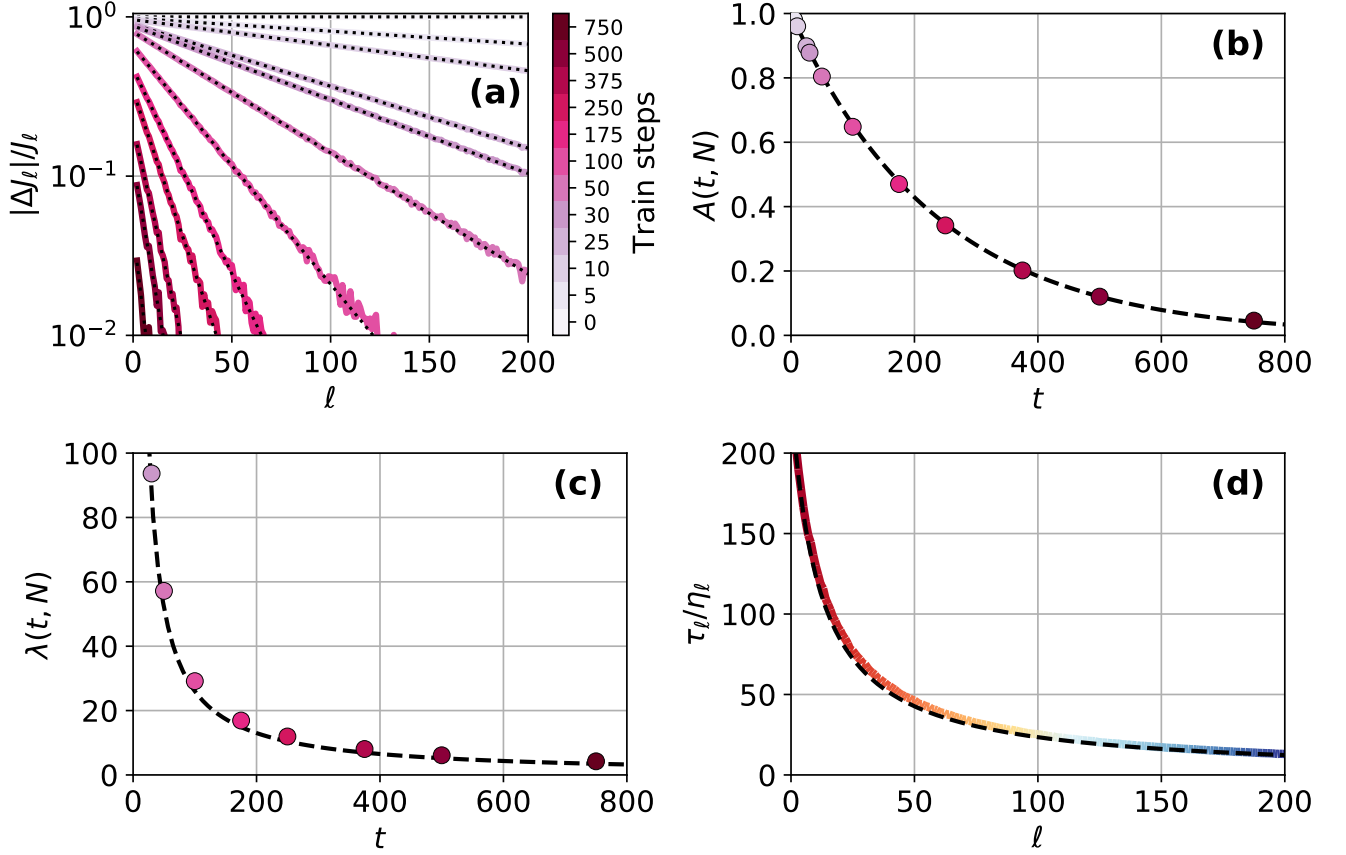


FIG. 5. Comparison between theory and numerical results for different quantities. The data used come from the same training of Fig. 4. (a) Relative error $|\Delta J_\ell|/J_\ell$ plotted as a function of ℓ , together with an exponential fit to the form $Ae^{-\frac{t}{\lambda}}$ (dashed black lines). (b,c) The values of the fitted parameters A and λ (data points) are compared with those derived from the theory (dashed black lines). (d) The effective timescale $\hat{\tau}_\ell = \tau_\ell/\eta_\ell$, obtained fitting the relative error as $\frac{|\Delta J_\ell|}{J_\ell} = e^{-\frac{t}{\hat{\tau}_\ell}}$, is compared to the prediction from the theory.

architectures. This analysis is left for future work.

B. Analysis of Global Annealing and first passage times

We are interested in the time taken by the system to generate a configuration of a given (absolute) magnetization. Therefore, we can consider the dynamics of the model in the space of (intensive) magnetizations, which can be described in terms of a simple one-dimensional Markov chain. Then, we consider the time required by the chain to first reach a magnetization equal or greater (possibly in modulus) than a target magnetization. At fixed β , we take as the target magnetization the equilibrium magnetization, i.e. the solution m^* of Eq. (3).

We start by noting that the average first-transition times $\tau_{m \rightarrow m^*}$ for going from a magnetization m to a magnetization m^* can be obtained using the set of self-consistent equations [46]:

$$\tau_{m \rightarrow m^*} = 1 + \sum_{\hat{m} \neq m^*} P(m \rightarrow \hat{m}) \tau_{\hat{m} \rightarrow m^*}, \quad m \neq m^*. \quad (28)$$

If we call $\boldsymbol{\tau}$ the vector of the average first passage times (excluding the first passage time $m^* \rightarrow m^*$) and \mathbb{Q} the matrix of the transition probabilities with the row and column corresponding to m^* removed, we can rewrite the system in matrix form as:

$$(\mathbb{I} - \mathbb{Q})\boldsymbol{\tau} = \mathbf{1}, \quad (29)$$

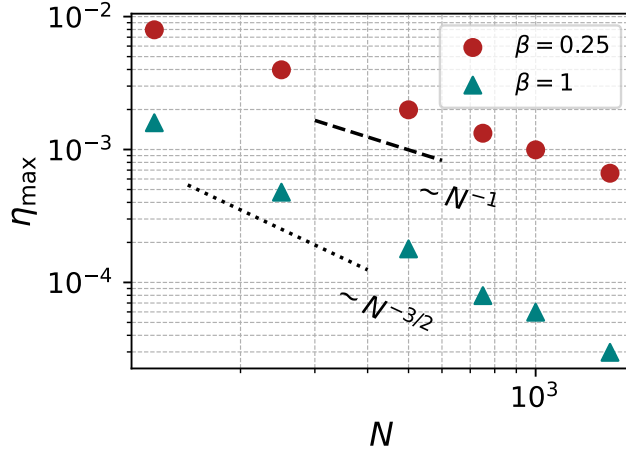


FIG. 6. Maximum learning rate η_{\max} as a function of system size N at high temperature ($\beta = 0.25$) and at criticality ($\beta = 1$). The black segments highlight the scaling laws. The maximum learning rate is estimated by evaluating GD convergence as follows: we start from zero couplings, perform two numerical GD steps (using 50 000 equilibrium configurations), and check whether the couplings remain positive (negative couplings after two GD steps indicate that GD does not converge). We then perform a bisection search to find the largest learning rate that still allows convergence.

where \mathbb{I} is the identity matrix and $\mathbf{1}$ is the vector of all ones. In practice, since we are interested in reaching magnetizations $m \geq m^*$, Eq. (28) reduces to

$$\tau_{m \rightarrow m^*} = 1 + \sum_{\hat{m} < m^*} P(m \rightarrow \hat{m}) \tau_{\hat{m} \rightarrow m^*}, \quad m \neq m^*, \quad (30)$$

and therefore the size of the matrix that needs to be effectively inverted is smaller. We will use signed magnetizations for the comparison with standard LMMC in Sec. IV C. In Sec. IV A and IV B we will use the absolute values instead. Equation (30) stays the same but in terms of absolute magnetizations $|m|$ instead of signed magnetizations m . The transition matrix in (30) is then further reduced by looking at the space of absolute magnetizations and, therefore, at the transition times to reach $|m| \geq |m^*|$.

Notice that, if the matrix $\mathbb{I} - \mathbb{Q}$ is tridiagonal (as in the case for local single-spin flip algorithms), Eq. (29) can be solved in linear time, either by inverting the matrix [47, 48], or using Thomas' algorithm [49, 50].

We point out that, in alternative to the described procedure, one could evaluate the equilibration time also by looking at the second largest eigenvalues of the probability transition matrix. The advantage of looking at first passage times, however, is that if m is not too large, one can work with an effective matrix that is smaller than the original one, thus making the computation easier.

We consider three Monte Carlo schemes, in which:

- only MADE global steps are performed;
- only LMMC steps are performed;
- a MADE step is followed by one or more LMMC sweeps.

An example of a comparison of the first passage times obtained by the analytical procedure described above and those obtained by performing a simulation in the case in which a MADE step is followed by one LMMC sweep is shown in Fig. 7. Just for this plot, we did not fix the target magnetization as the equilibrium one, but instead fixed $\beta = 1.1$ and considered different values of m . We stress that it is possible to reach magnetizations larger than the equilibrium one since we are considering a finite-size system, so that the probability of reaching an arbitrarily large magnetization by a random fluctuation is always non-zero.

The transition matrices obtained in the three cases are described in the following sections.

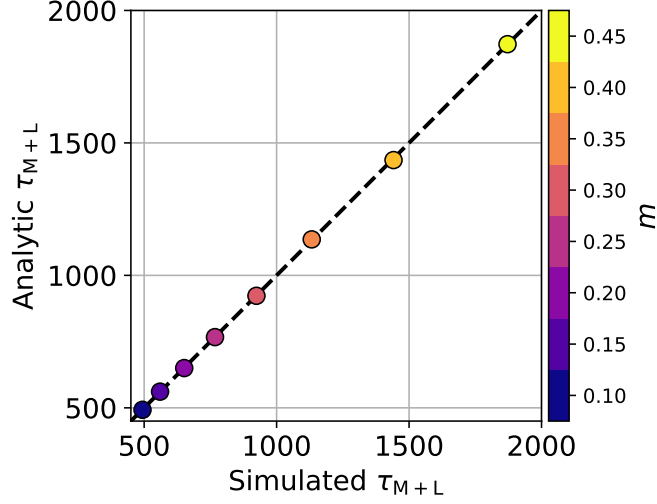


FIG. 7. Comparison between the first passage times it takes for the procedure that alternates a global MADE move and a local MCS to reach magnetization m starting from zero magnetization, τ_{M+L} (where M+L stands for MADE+LMMC). The values computed analytically are plotted versus those obtained numerically. Data are for $N = 200$ and $\beta = 1.1$. The averages are performed over $5 \cdot 10^4$ runs. Both times were multiplied by $2N$ to take into account the computational complexity of each move.

1. Local Metropolis Monte Carlo

We recall that for the single-spin-flip Metropolis MC one selects one spin at random and flips it with probability:

$$\text{Acc}[\boldsymbol{\sigma} \rightarrow \boldsymbol{\sigma}'] = \min[1, e^{-\beta\Delta E}] . \quad (31)$$

Let us consider a configuration with magnetization m and suppose one randomly selects a spin σ . The change in energy if the spin is flipped is:

$$\Delta E = -2 \left(\frac{1}{N} - \sigma m \right) . \quad (32)$$

If $m = 0$, $\Delta E < 0$ and the move is always accepted. When $|m| > 0$ and one selects a spin at random, the probability of it having a sign opposite to m is $\frac{1-|m|}{2}$ (and that of having the same sign is $\frac{1+|m|}{2}$). Using this and equations (31) and (32), we can write the transition probability of the Markov chain, keeping in mind that, since the dynamic is local, jumps in magnetization only occur between configurations separated by $\Delta m = 2/N$:

$$P(m \rightarrow m') = \begin{cases} P(m \rightarrow m - \frac{2}{N}) = \frac{1+m}{2} \min[1, \exp(-2\beta(m - \frac{1}{N}))], \\ P(m \rightarrow m + \frac{2}{N}) = \frac{1-m}{2} \min[1, \exp(2\beta(m + \frac{1}{N}))], \\ P(m \rightarrow m) = 1 - \frac{1+m}{2} \min[1, \exp(-2\beta(m - \frac{1}{N}))] - \frac{1-m}{2} \min[1, \exp(2\beta(m + \frac{1}{N}))]. \end{cases} \quad (33)$$

Analogously, the transition matrix in the space of absolute magnetizations $|m|$ is:

$$P(|m| \rightarrow |m'|) = \begin{cases} P(0 \rightarrow \frac{2}{N}) = 1, & \text{for } |m| = 0, \\ \begin{cases} P(|m| \rightarrow |m| + \frac{2}{N}) = \frac{1-|m|}{2}, \\ P(|m| \rightarrow |m| - \frac{2}{N}) = \frac{1+|m|}{2} e^{-2\beta(|m| - \frac{1}{N})}, \\ P(|m| \rightarrow |m|) = 1 - \left(\frac{1-|m|}{2} + \frac{1+|m|}{2} e^{-2\beta(|m| - \frac{1}{N})} \right), \end{cases} & \text{for } |m| > 0, \\ P(|m| \rightarrow |m'|) = 0, & |m - m'| \neq 0, 2/N. \end{cases} \quad (34)$$

Interestingly, taking the $N \rightarrow \infty$ limit and requiring the probabilities of increasing and decreasing the magnetization to be equal yields:

$$\frac{1 + |m|}{2} e^{-2\beta|m|} = \frac{1 - |m|}{2} \quad \Leftrightarrow \quad |m| = \tanh \beta|m| , \quad (35)$$

which is the correct equation for the equilibrium magnetization in the Curie-Weiss model, Eq. (3).

2. MADE

The transition matrix in the case of the MADE can be written as:

$$P(|m| \rightarrow |m'|) = \begin{cases} \frac{\Omega(|m'|)}{\Omega(|m|)} \min\left(1, \frac{p_{\text{MADE}}(|m'|)}{p_{\text{MADE}}(|m|)} e^{\frac{\beta N}{2}(|m'|^2 - |m|^2)}\right) p_{\text{MADE}}(|m'|), & |m| \neq |m'|, \\ 1 - \sum_{|m''| \neq |m|} P(|m| \rightarrow |m''|), & |m| = |m'|, \end{cases} \quad (36)$$

where $\Omega(|m|)$ is the degeneracy of state $|m|$ and $p_{\text{MADE}}(|m|)$ is the probability that the MADE generates a configuration of magnetization $|m|$, which can be computed in a time $\mathcal{O}(N)$ given the weights. The transition matrix for the signed magnetizations is similar and can be computed analogously.

3. MADE and local Metropolis

Finally, if we consider a global step followed by k MCS, the transition matrix $\mathbb{P}_{\text{M+L}}$ will be simply given by the product

$$\mathbb{P}_{\text{M+L}} = \mathbb{P}_{\text{M}} \mathbb{P}_{\text{L}}^{kN}, \quad (37)$$

where \mathbb{P}_{L} and \mathbb{P}_{M} are the transition matrices defined in the previous sections for the LMMC and MADE, respectively. In the following, we will always take $k = 1$ for simplicity.

In Sec. IV, we compare the first passage times for the different methods to determine which procedure is the fastest to reach the target magnetization.

IV. RESULTS

In order to assess the relevance of adding LMMC to global NN-assisted moves, we consider the following setting, which corresponds to a single temperature jump in the GA procedure. We suppose that a NN has been trained (either perfectly or not) at the critical temperature T_c of the model, where the spontaneous magnetization is still zero. Then, we want to use the NN to perform NN-assisted MC at a temperature $T < T_c$ below the critical temperature, at which $m^* \neq 0$. We compare the dynamics with global MADE moves only (indicated by M for MADE) with the dynamics with global MADE moves and LMMC (indicated by M+L for MADE+LMMC), and compare the time it takes for the two dynamics to reach equilibrium, i.e. to reach m^* .

A. Perfectly trained MADE

We first consider a perfectly trained MADE, i.e., a MADE with weights given by the solution to Eq. (11) at the critical temperature $\beta_c = 1$ (we recall that these weights are non-zero at finite N). We then evaluate the times required to reach the absolute equilibrium magnetization $|m^*|$ given by Eq. (3) at inverse temperature $\beta \geq \beta_c$ (i.e. below the critical temperature) starting from zero magnetization, and we consider the ratio

$$R = \frac{2\tau_{\text{M+L}}}{\tau_{\text{M}}}, \quad (38)$$

where τ_{M} and $\tau_{\text{M+L}}$ are the average first passage times for the two procedures and the factor two takes into account the fact that performing both a global move and a MCS takes approximately twice the number of operations as performing just a global move. Hence, $R > 1$ indicates that the MADE by itself is more efficient than MADE+LMMC, while $R < 1$ indicates that adding local moves is beneficial.

We first show in Fig. 8 the results for different β . The curves start at $R = 2$ for $\Delta\beta = \beta - \beta_c \simeq 0$, signaling that the perfectly trained NN is good enough to generate the target magnetization even on its own, without the need for local MC steps. Because the NN is good enough to generate configurations with the desired magnetization, adding LMMC on top of the global moves only adds to the computational time. Upon increasing $\Delta\beta$, as the machine is used at temperatures that are further away from the one at which it was trained, R drops and it becomes increasingly necessary to add LMMC. The transition between these two regimes, however, moves at lower $\Delta\beta$ as N increases. In particular, as shown in Fig. 8b, the curves collapse when plotted as a function of $\Delta\beta\sqrt{N}$. Therefore, as long as the temperature step is chosen as $\Delta\beta = b/\sqrt{N}$ with b small enough, a typical annealing schedule in practical applications,

adding MC moves is actually not helpful. However, already for $b \gtrsim 1.5$ (which is not an uncommon choice), the LMMC clearly improves the performances of the MADE. Moreover, this analysis does not take into account the (non-negligible) computational cost of training the MADE. Considering also the training time, the scenario changes, as we show in the following section.

B. Partially trained MADE

We now turn to the case in which the MADE is not already pre-trained and all the weights are initialized to zero. This setting introduces a tradeoff in the training time: on the one hand, longer training is computationally more expensive; on the other hand, untrained weights make the performance worse (e.g. at initialization all weights are zero and the MADE simply extracts one configuration uniformly at random from the 2^N possible ones). While it is unclear, *a priori*, which is the optimal training time t , we can track the evolution of the weights as a function of the number of training steps using Eq. (25) and compute the average first passage times as in the previous section. Following the discussion in Sec. III A 3, we fix the learning rate $\eta = N^{-\frac{3}{2}}$.

We plot R at fixed $b = 0.5$ as a function of the training time in Fig. 9a. From Fig. 8b, for $b = 0.5$ we expect $R_\infty \sim 1.6$ at infinite training time, which is confirmed by Fig. 9a. We see that, at finite training time, the performance of the MADE alone deteriorates with respect to MADE+LMMC, i.e. $R < R_\infty$. This phenomenon is even more evident Fig. 9b where we considered a modification of Eq. (38) that takes into account the training time T_t (considering that each epoch takes $\sim N$ steps), i.e. the ratio

$$\hat{R} = \frac{2\tau_{M+L} + T_t}{\tau_M + T_t}. \quad (39)$$

Performing LMMC helps, because it gives a huge hand when MADE is not trained enough, and even when MADE is good enough to be used alone, the addition of the training time adds an overhead that dominates over the additional cost of performing LMMC, so that the ratio remains always close to one or below.

We thus conclude that, if one has equilibrated at the critical temperature and wants to equilibrate within one of the two states that appear just below it, MADE+LMMC is generically more efficient than MADE alone.

C. Comparison with local Metropolis Monte Carlo

Having assessed that MADE+LMMC is more efficient than MADE alone, one might wonder whether the MADE is needed at all. To answer this question, we compare in the same setting the MADE+LMMC dynamics with that with LMMC only. The first passage time ratio

$$R' = \frac{2\tau_{M+L} + T_t}{\tau_L}. \quad (40)$$

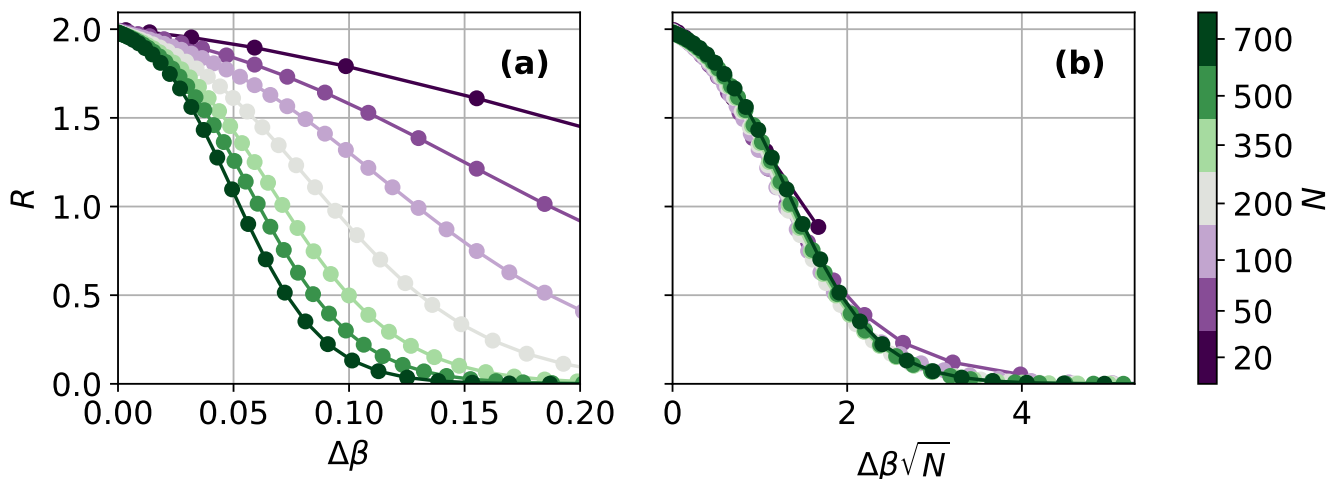


FIG. 8. Ratio R of first passage times as a function of $\Delta\beta = \beta - \beta_c$ (a) and of $\Delta\beta\sqrt{N}$ (b).

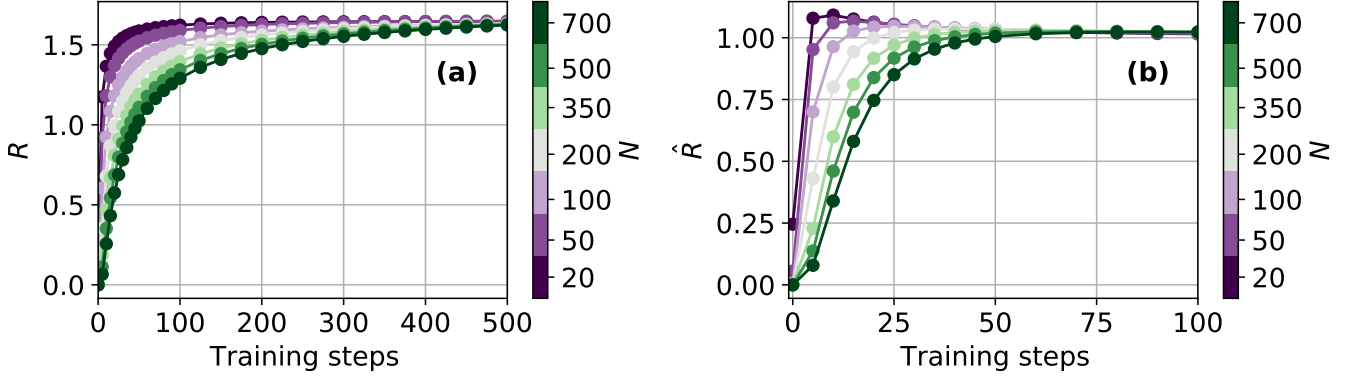


FIG. 9. (a) Ratios of the average first passage time R (not taking account training) and (b) \hat{R} (taking account training) at $\Delta\beta = b/\sqrt{N}$ with $b = 0.5$. The learning rate is fixed to $\eta = N^{-\frac{3}{2}}$.

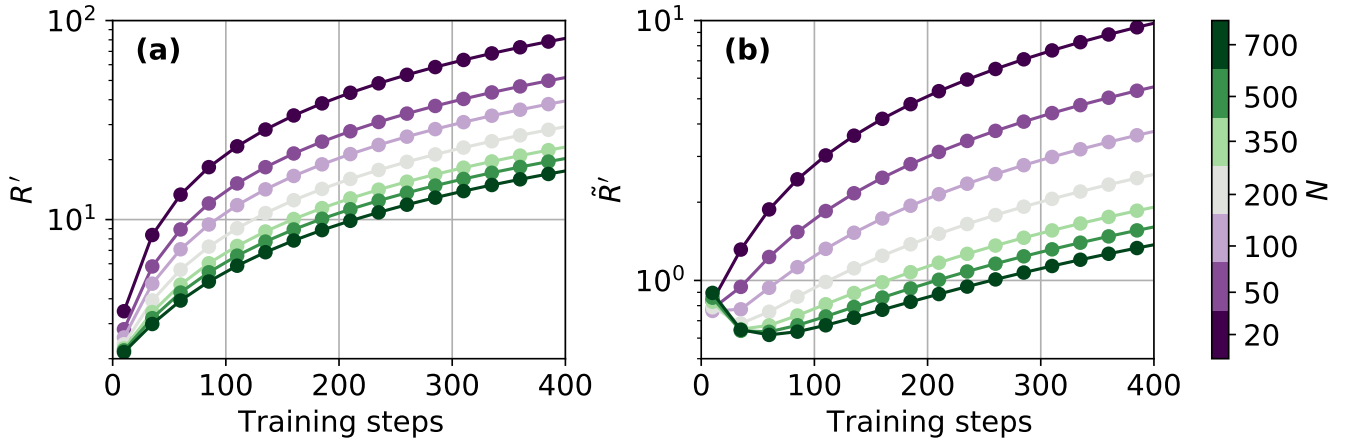


FIG. 10. (a) Ratio R' of the average first passage time between the MADE+LMMC (including training time) and the LMMC alone, for the absolute value of magnetization, as a function of training time for fixed $\Delta\beta = b/\sqrt{N}$ with $b = 2$. (b) Same plot for the ratio \tilde{R}' for the signed value of the magnetization. The learning rate is fixed to $\eta = N^{-\frac{3}{2}}$.

is shown in Fig. 10a and it turns out that simply using just LMMC performs better, i.e. we always observe that $R' > 1$.

This is due to the fact that we are only considering the absolute value of the magnetization: the addition of the MADE helps in exploring better the energy landscape by allowing sudden jumps between the two states that are present at $T < T_c$. This can be seen in Fig. 10b, in which we considered the ratio

$$\tilde{R}' = \frac{2\tilde{\tau}_{M+L} + T_t}{\tilde{\tau}_L} \quad (41)$$

where $\tilde{\tau}_L$ and $\tilde{\tau}_{M+L}$ are the average first passage times of LMMC and MADE+LMMC for reaching the signed (positive) equilibrium magnetization starting from zero magnetization. In this case, we observe that $\tilde{R}' < 1$, indicating a better efficiency of MADE+LMMC, when N is sufficiently large and the number of training steps is not too high (otherwise, the computational cost outweighs the gains from using MADE). The LMMC alone has worse performance, because it can end up in the negative state and be stuck there for a long time. The addition of the MADE avoids this problem. Note that the barrier for LMMC to jump from the negative to the positive state scales as $\exp(AN\Delta\beta^2) = \exp(Ab^2)$, hence it remains finite with the chosen scaling of $\Delta\beta = b/\sqrt{N}$. When instead $\beta - \beta_c = O(1)$, the LMMC needs a time scaling exponentially in N , and the gain from using the MADE becomes even more visible. We expect a similar behavior to hold in the whole ferromagnetic region.

V. CONCLUSIONS

In this work, we were able to fully describe a generative autoregressive architecture, the shallow MADE, for the study of the Curie-Weiss model at finite size N . We first characterized the problem in terms of the optimal couplings that can be found in order to approximate the Curie-Weiss distribution. We were then able to describe how these couplings are learned during the training process. Interestingly, we found that the system undergoes a critical slowing down in the learning characterized by the same behavior as typical local dynamics. Further work is needed to test whether this is a general result or a peculiarity of the model.

We were then able to use these results to benchmark the model performances with and without additional local Monte Carlo steps in the Global Annealing procedure. We found that using the perfectly trained architecture renders additional local Monte Carlo steps unnecessary, as long as a suitable annealing schedule is chosen (i.e. with small enough $b = \Delta\beta\sqrt{N}$). However, since the cost of training the architecture increases with the model size, one has to resort to using an imperfectly trained machine, which in turn benefits from using additional local Monte Carlo steps. However, we verified that the NN-assisted procedure is actually able to outperform that with local moves only because it allows jumping between distinct states that form below the critical temperature, thus showing the improvement coming from the usage of the architecture. In summary, the NN role is mostly to allow for efficient sampling of distinct states, while the local moves are mostly needed to efficiently sample within a state.

Based on these results we predict that, in practical applications, the use of generative autoregressive NN is helpful to better simulate the systems of interest whenever more than one state is present. However, since in practice one has to compromise between the accuracy and time of training, the addition of Monte Carlo steps will actually improve the results. Further numerical tests of these ideas are left for future work.

CODE AVAILABILITY

The code used in this paper is available at the GitHub repository [51].

ACKNOWLEDGMENTS

We thank Giulio Biroli, Marylou Gabri e and Guilhem Semerjian for useful discussions. The research has received financial support from the ‘‘National Centre for HPC, Big Data and Quantum Computing - HPC’’, Project CN_00000013, CUP B83C22002940006, NRP Mission 4 Component 2 Investment 1.4, Funded by the European Union - NextGenerationEU. Author LMDB acknowledges funding from the Bando Ricerca Scientifica 2024 - *Avvio alla Ricerca* (D.R. No. 1179/2024) of Sapienza Universit a di Roma, project B83C24005280001 – MaLeDiSSi. We acknowledge support from the computational infrastructure DARIAH.IT, PON Project code PIR01_00022, National Research Council of Italy.

-
- [1] Marc M ezard, Giorgio Parisi, and Miguel Angel Virasoro. *Spin Glass Theory and Beyond*. World Scientific, 1987.
 - [2] Daniel L. Stein and Charles M. Newman. Applications to other fields. In *Spin Glasses and Complexity*. Princeton University Press, 01 2013.
 - [3] Patrick Charbonneau, Enzo Marinari, Giorgio Parisi, Federico Ricci-Tersenghi, Gabriele Sicuro, Francesco Zamponi, and Marc Mezard. *Spin glass theory and far beyond: replica symmetry breaking after 40 years*. World Scientific, 2023.
 - [4] Koji Hukushima and Koji Nemoto. Exchange monte carlo method and application to spin glass simulations. *Journal of the Physical Society of Japan*, 65(6):1604–1608, 1996.
 - [5] J er ome Houdayer. A cluster monte carlo algorithm for 2-dimensional spin glasses. *The European Physical Journal B-Condensed Matter and Complex Systems*, 22:479–484, 2001.
 - [6] Zheng Zhu, Andrew J Ochoa, and Helmut G Katzgraber. Efficient cluster algorithm for spin glasses in any space dimension. *Physical review letters*, 115(7):077201, 2015.
 - [7] Koji Hukushima and Yukito Iba. Population annealing and its application to a spin glass. In *AIP Conference Proceedings*, volume 690, pages 200–206. American Institute of Physics, 2003.
 - [8] Jonathan Machta. Population annealing with weighted averages: A monte carlo method for rough free-energy landscapes. *Physical Review E—Statistical, Nonlinear, and Soft Matter Physics*, 82(2):026704, 2010.
 - [9] Wenlong Wang, Jonathan Machta, and Helmut G Katzgraber. Comparing monte carlo methods for finding ground states of ising spin glasses: Population annealing, simulated annealing, and parallel tempering. *Physical Review E*, 92(1):013303, 2015.

- [10] Lev Yu Barash, Martin Weigel, Michal Borovský, Wolfhard Janke, and Lev N Shchur. Gpu accelerated population annealing algorithm. *Computer Physics Communications*, 220:341–350, 2017.
- [11] Martin Weigel, Lev Barash, Lev Shchur, and Wolfhard Janke. Understanding population annealing monte carlo simulations. *Physical Review E*, 103(5):053301, 2021.
- [12] Piotr Białas, Piotr Korcyl, and Tomasz Stebel. Hierarchical autoregressive neural networks for statistical systems. *Computer Physics Communications*, 281:108502, 2022.
- [13] Simone Ciarella, Jeanne Trinquier, Martin Weigt, and Francesco Zamponi. Machine-learning-assisted monte carlo fails at sampling computationally hard problems. *Machine Learning: Science and Technology*, 4(1):010501, 2023.
- [14] Indaco Biazzo, Dian Wu, and Giuseppe Carleo. Sparse autoregressive neural networks for classical spin systems. *Machine Learning: Science and Technology*, 2024.
- [15] Luca Maria Del Bono, Federico Ricci-Tersenghi, and Francesco Zamponi. Nearest-neighbours neural network architecture for efficient sampling of statistical physics models. *arXiv preprint arXiv:2407.19483*, 2024.
- [16] Christoph Schönle and Marylou Gabrié. Optimizing markov chain monte carlo convergence with normalizing flows and gibbs sampling. In *NeurIPS 2023 AI for Science Workshop*, 2023.
- [17] Kim A Nicoli, Christopher J Anders, Tobias Hartung, Karl Jansen, Pan Kessel, and Shinichi Nakajima. Detecting and mitigating mode-collapse for flow-based sampling of lattice field theories. *Physical Review D*, 108(11):114501, 2023.
- [18] Giulio Biroli and Marc Mézard. Generative diffusion in very large dimensions. *Journal of Statistical Mechanics: Theory and Experiment*, 2023(9):093402, 2023.
- [19] Stefano Bae, Enzo Marinari, and Federico Ricci-Tersenghi. A very effective and simple diffusion reconstruction for the diluted ising model. *arXiv preprint arXiv:2407.07266*, 2024.
- [20] Nicholas T Hunt-Smith, Wally Melnitchouk, Felix Ringer, Nobuo Sato, Anthony W Thomas, and Martin J White. Accelerating markov chain monte carlo sampling with diffusion models. *Computer Physics Communications*, 296:109059, 2024.
- [21] Aurélien Decelle, Beatriz Seoane, Lorenzo Rosset, Cyril Furtlehner, Nicolas Berez, Giovanni Catania, and Elisabeth Agoritsas. The restricted boltzmann machine: from the statistical physics of disordered systems to a practical and interpretative generative machine learning. *Bulletin of the American Physical Society*, 2024.
- [22] Tanguy Marchand, Misaki Ozawa, Giulio Biroli, and Stéphane Mallat. Wavelet conditional renormalization group. *arXiv preprint arXiv:2207.04941*, 2022.
- [23] Kanta Masuki and Yuto Ashida. Generative diffusion model with inverse renormalization group flows. *arXiv preprint arXiv:2501.09064*, 2025.
- [24] Leonardo Galliano, Riccardo Rende, and Daniele Coslovich. Policy-guided monte carlo on general state spaces: Application to glass-forming mixtures. *The Journal of Chemical Physics*, 161(6), 2024.
- [25] Daria Pugacheva, Andrei Ermakov, Igor Lyskov, Ilya Makarov, and Yuriy Zotov. Enhancing gnns performance on combinatorial optimization by recurrent feature update. *arXiv preprint arXiv:2407.16468*, 2024.
- [26] Zi-Song Shen, Feng Pan, Yao Wang, Yi-Ding Men, Wen-Biao Xu, Man-Hong Yung, and Pan Zhang. Free-energy machine for combinatorial optimization. *Nature Computational Science*, pages 1–11, 2025.
- [27] Dian Wu, Lei Wang, and Pan Zhang. Solving statistical mechanics using variational autoregressive networks. *Physical review letters*, 122(8):080602, 2019.
- [28] Giuseppe Carleo and Matthias Troyer. Solving the quantum many-body problem with artificial neural networks. *Science*, 355(6325):602–606, 2017.
- [29] B McNaughton, MV Milošević, A Perali, and S Pilati. Boosting monte carlo simulations of spin glasses using autoregressive neural networks. *Physical Review E*, 101(5):053312, 2020.
- [30] Marylou Gabrié, Grant M Rotskoff, and Eric Vanden-Eijnden. Adaptive monte carlo augmented with normalizing flows. *Proceedings of the National Academy of Sciences*, 119(10):e2109420119, 2022.
- [31] Shams Mehdi, Zachary Smith, Lukas Herron, Ziyue Zou, and Pratyush Tiwary. Enhanced sampling with machine learning. *Annual Review of Physical Chemistry*, 75, 2024.
- [32] Leticia F Cugliandolo and Jorge Kurchan. Analytical solution of the off-equilibrium dynamics of a long-range spin-glass model. *Physical Review Letters*, 71(1):173, 1993.
- [33] Federico Ricci-Tersenghi. Being glassy without being hard to solve. *Science*, 330(6011):1639–1640, 2010.
- [34] Andrea Montanari and Federico Ricci-Tersenghi. Cooling-schedule dependence of the dynamics of mean-field glasses. *Physical Review B—Condensed Matter and Materials Physics*, 70(13):134406, 2004.
- [35] Giampaolo Folena, Silvio Franz, and Federico Ricci-Tersenghi. Rethinking mean-field glassy dynamics and its relation with the energy landscape: The surprising case of the spherical mixed p-spin model. *Physical Review X*, 10(3):031045, 2020.
- [36] Carlo Baldassi, Clarissa Lauditi, Enrico M Malatesta, Gabriele Perugini, and Riccardo Zecchina. Unveiling the structure of wide flat minima in neural networks. *Physical Review Letters*, 127(27):278301, 2021.
- [37] Andrew Ly and Pulin Gong. Optimization on multifractal loss landscapes explains a diverse range of geometrical and dynamical properties of deep learning. *Nature Communications*, 16(1):3252, 2025.
- [38] Indaco Biazzo. The autoregressive neural network architecture of the boltzmann distribution of pairwise interacting spins systems. *Communications Physics*, 6(1):296, 2023.
- [39] Sacha Friedli and Yvan Velenik. *Statistical mechanics of lattice systems: a concrete mathematical introduction*. Cambridge University Press, 2018.
- [40] Mark EJ Newman and Gerard T Barkema. *Monte Carlo methods in statistical physics*. Clarendon Press, 1999.
- [41] Fernando Martínez-García and Diego Porras. Problem hardness of diluted ising models: Population annealing vs simulated annealing. *arXiv preprint arXiv:2501.07638*, 2025.

- [42] Mathieu Germain, Karol Gregor, Iain Murray, and Hugo Larochelle. Made: Masked autoencoder for distribution estimation. In *International conference on machine learning*, pages 881–889. PMLR, 2015.
- [43] Pankaj Mehta, Marin Bukov, Ching-Hao Wang, Alexandre GR Day, Clint Richardson, Charles K Fisher, and David J Schwab. A high-bias, low-variance introduction to machine learning for physicists. *Physics reports*, 810:1–124, 2019.
- [44] Aydin Deger and Christian Flindt. Lee-yang theory of the curie-weiss model and its rare fluctuations. *Physical Review Research*, 2(3):033009, 2020.
- [45] Joris Bierkens and Gareth Roberts. A piecewise deterministic scaling limit of lifted metropolis–hastings in the curie–weiss model. *The Annals of Applied Probability*, 27(2):846–882, 2017. Accessed 7 May 2025.
- [46] Jeffrey J Hunter. The computation of the mean first passage times for markov chains. *Linear Algebra and its Applications*, 549:100–122, 2018.
- [47] Riaz A Usmani. Inversion of a tridiagonal jacobi matrix. *Linear Algebra and its Applications*, 212(213):413–414, 1994.
- [48] CM Da Fonseca. On the eigenvalues of some tridiagonal matrices. *Journal of Computational and Applied Mathematics*, 200(1):283–286, 2007.
- [49] Llewellyn Hilleth Thomas. Elliptic problems in linear difference equations over a network. *Watson Sci. Comput. Lab. Rept., Columbia University, New York*, 1:71, 1949.
- [50] Min Tian, Qi Liu, Jingshan Pan, Ying Gou, and Zanjun Zhang. swpts: an efficient parallel thomas split algorithm for tridiagonal systems on sunway manycore processors. *The Journal of Supercomputing*, 80(4):4682–4706, 2024.
- [51] Code available at: https://github.com/Laplaxe/MonteCarloGA_CW.